A Comparative Study of TiO_2 and Surface-Treated TiO_2 Nanoparticles on Thermal and Mechanical Properties of Poly(ε-caprolactone) Nanocomposites

Guangshuo Wang,[1] Guangyi Chen,[2] Zhiyong Wei,[2] Teng Yu,[3] Lian Liu,[3] Pei Wang,[3] Ying Chang,[2] Min Qi[1]

[1]*School of Material Science and Engineering, Dalian University of Technology, Dalian 116024, China*
[2]*School of Automotive Engineering, Dalian University of Technology, Dalian 116024, China*
[3]*School of Transportation Equipments and Ocean Engineering, Dalian Maritime University, Dalian 116026, China*

Received 1 August 2011; accepted 28 December 2011
DOI 10.1002/app.36720
Published online in Wiley Online Library (wileyonlinelibrary.com).

ABSTRACT: Polymer/inorganic nanocomposites were significant hybrid materials because of their unique properties. The surface of bare nanoparticles (b-TiO_2) was modified by aminopropyl trimethoxy silane to obtain grafted TiO_2 (g-TiO_2) nanoparticles for the improvement of nanoparticles dispersion. The b-TiO_2 and resulting g-TiO_2 nanoparticles were introduced into poly(ε-caprolactone) (PCL) matrix to prepare PCL/TiO_2 nanocomposites by *in situ* polymerization. The effects of b-TiO_2 and g-TiO_2 nanoparticles on the structure, morphology, and properties of nanocomposites were characterized and compared. The results showed that the crystalline structure of PCL matrix was not affected significantly by adding b-TiO_2 or g-TiO_2 nanoparticles. The g-TiO_2 nanoparticles had a finer dispersion and better compatibility than bare TiO_2. The introduction of g-TiO_2 into PCL matrix increased the crystallization temperature and improved thermal stability of the nanocomposites with respect to untreated TiO_2. The surface-treated nanoparticles played an important role in strengthening mechanical properties of the nanocomposites because of its well dispersion and strong interfacial interaction between the nanoparticles and PCL matrix. © 2012 Wiley Periodicals, Inc. J Appl Polym Sci 000: 000–000, 2012

Key words: poly(ε-caprolactone); surface-treated TiO_2; nanocomposites; thermal properties; mechanical properties

INTRODUCTION

The development of biodegradable polymers derived from renewable natural materials has received considerable attention, and they have already found many applications in market areas. Poly(ε-caprolactone) (PCL), having many excellent properties, such as fully biodegradable and biocompatible, nontoxic to living organisms, tailorable degradation kinetics, is one of the most promising candidates of these kinds of biodegradable polymers[1] and has a great potential in medical applications, including controlled drug-delivery system, surgical sutures and tissue engineering scaffolds, and other long-term degradable implants.[2] However, the application of PCL might be limited in that its disadvantages in mechanical strength, thermal stability, gas permeability, solvent resistance, hydrophobic character, and slower degradation rate compared with other polylactones.[3] One promising alternative is to prepare nanocomposites by the combination of an environmentally acceptable filler to improve the properties of such biodegradable polymers to meet the rapid development in some special applications.[4]

A wide range of nanocomposites are being developed in the recent years. Polymer/inorganic nanocomposites combining the advantages of both the organic polymer and inorganic component have been studied intensively.[5–10] Among inorganic nanoparticles, titanium dioxide (TiO_2) has been extensively investigated as reinforcement filler for thermoplastics, such as poly(vinyl chloride) (PVC),[11,12] polypropylene (PP),[13] polystyrene (PS),[14] etc. Moreover, TiO_2 nanoparticles have found many versatile functions such as attractive photocatalytic, far-infrared radiation, antibacterial properties, and UV-resistance because of its robust and general reactivity.[15] As we know, the final properties of nanocomposites depend strongly on the particle shape, particle size, aggregate size, surface characteristics, and degree of dispersion, and the key is to achieve good homogeneity of the nanoparticles dispersion for high

Correspondence to: Z. Wei (zywei@dlut.edu.cn) or M. Qi (minqi@dlut.edu.cn).

Contract grant sponsor: National Natural Science Foundation of China; contract grant numbers: 30870633, 31000427, 50901011.
Contract grant sponsor: National High Technology Research and Development Program of China; contract grant number: 2009AA03Z319.
Contract grant sponsor: Fundamental Research Funds for the Central Universities.

performances. It is of difficultly to control the dispersion of nanoparticles, though property improvements (stiffness, thermal stability, lower permeability, etc.) have been obtained in PCL/TiO_2 nanocomposites.[16–18] To achieve a proper dispersion of nanoparticles within polymer matrix and a better compatibility between the nanoparticles and host polymer, the use of coupling agents such as aminopropyl trimethoxy silane (APS) for surface modification of nanoparticles is recommended.[19]

In this study, PCL/TiO_2 nanocomposites were prepared by *in situ* polymerization of ε-caprolactone (ε-CL) in the presence of untreated or surface-treated TiO_2. The effects of untreated TiO_2 and surface-treated TiO_2 nanoparticles on the structure, morphology, and properties of PCL/TiO_2 nanocomposites were fully investigated.

EXPERIMENTAL

Materials

ε-CL (99%, Acros Organics, Belgium) was dried over CaH_2 by stirring and distilled under reduced pressure prior to use. Tin 2-ethylhexamoate ($Sn(Oct)_2$, >95%, Sigma-Aldrich, St. Louis, MO) was used as catalyst of ring opening polymerization (ROP) of ε-CL. Aminopropyl trimethoxy silane (APS, 97%, Sigma-Aldrich, St. Louis, MO) and triethyl amine (Et_3N, 99%, Sigma-Aldrich, St. Louis, MO) were used as coupling agent and surface grafting catalyst. Anatase TiO_2 nanoparticles were purchased from Wanjing New Material (Hangzhou, China) under the trade name VK-TA03, having a specific surface area of 100–250 m^2/g, and average primary particle size of 20–30 nm. Other chemical reagents were analytical grade and used as received.

Surface modification of TiO_2 nanoparticles

TiO_2 (10 g) nanoparticles were kept in a vacuum chamber for 24 h at 100°C, and then ultrasonically dispersed in 500 mL butanone for 30 min. The suspension was then stirred for a further 1 h. The mixture was mixed with a 300 mL of butanone solution of APS (2.4 g) and 1.5 mL of triethyl amine. The suspension was refluxed for 3 h at 80°C and then cooled to room temperature. After centrifugal separation, the nanoparticles were finally dried in a low pressure at 80°C for 12 h. And the resulting nanoparticles were named as g-TiO_2 and the bare TiO_2 nanoparticles were named as b-TiO_2.

Preparation of PCL/TiO_2 nanocomposites

The polymerization of ε-CL was carried out via the ROP with the OH groups on the surface of TiO_2 nanoparticles as initiators and $Sn(Oct)_2$ as catalyst. The same procedure was applied in both surface-treated TiO_2 and untreated TiO_2 nanoparticles. In a typical experiment, the desired amount of TiO_2 (0.1 g) was suspended in ε-CL (9.9 g) by means of ultrasonic treatment for 30 min, then the suspension including TiO_2, $Sn(Oct)_2$, and ε-CL was transferred to a three-necked flask, which was previously dried in vacuum oven at 140°C. The reaction flask was heated at 130°C for 10 h under magnetic stirring. Polymerization was stopped by rapid cooling to room temperature. The obtained products were dried in a vacuum at 40°C for 24 h to remove the residual solvent. Corresponding to the feed weight percentage of TiO_2, the composites were designated as PCL (0 wt % TiO_2), PCL-b1 (1 wt % b-TiO_2), PCL-b3 (3 wt % b-TiO_2), PCL-b5 (5 wt % b-TiO_2), PCL-g1 (1 wt % g-TiO_2), PCL-g3 (3 wt % g-TiO_2), and PCL-g5 (5 wt % g-TiO_2).

Characterization

The Fourier transform infrared spectroscopy (FTIR) analysis was performed at room temperature using a Magna 750 spectrometer (Nicolet, USA). The spectra were recorded from 400 to 4000 cm^{-1} with a spectral resolution of 4 cm^{-1}. The grafted and non-grafted TiO_2 nanoparticles were mixed with KBr powders and pressed into flakes for FTIR measurements.

The wide-angle X-ray diffraction (WAXD) patterns of the samples were performed on a Dmax-Ultima+ X-ray diffractometer (Rigaku, Japan) with Ni-filtered Cu/K_α radiation ($\lambda = 0.15418$ nm). The operating target voltage was 40 kV and the tube current was 100 mA. The scanning speed was 1.2°/min from 5° to 70° for TiO_2 nanoparticles and 10° to 30° for PCL/TiO_2 nanocomposites.

The molecular weight and molecular weight distribution of PCL/TiO_2 nanocomposites were measured by GPC-220 (Polymer Laboratory, UK) equipped with Ultrastyragel® columns and differential refractometer. Tetrahydrofuran (THF) was used as an eluent at a flow rate of 1.0 mL/min at 40°C. The polymer molecular weights were obtained with narrow molecular weight distribution PS standards.

A FEI (Nanosem 430, HK) field emission scanning electron microscope (FESEM) was used to evaluate the cryofractured surfaces of PCL/TiO_2 nanocomposites. The samples were sputter coated with a thin layer of gold before the surface characterization. Accelerating voltages of 10 kV was used for the observation.

A JEOL (H-7650, Japan) transmission electron microscope (TEM) was utilized to observe the morphology of TiO_2 nanoparticles and PCL/TiO_2 nanocomposites. Before electron microscopy observation,

the nanocomposites were cut into thin pieces using an ultramicrotome.

Nonisothermal crystallizations of PCL/TiO_2 nanocomposites were performed in a DSC1 (Mettler-Toledo, Switzerland) differential scanning calorimeter. The instrument was calibrated using high-purity indium and zinc standards. Each sample (ca. 5 mg) was initially melted at 80°C for 5 min to erase the previous thermal history, and then the sample was cooled to 0°C at cooling rate of 10°C/min. After the completion of nonisothermal crystallization, the sample was subsequent heated to 80°C at 10°C/min, and the heat flows during both crystallization and melting process were recorded.

Thermal stability analysis of PCL/TiO_2 nanocomposites was performed by TGA/SDTA851 (Mettler, Switzerland). The measurements were performed at 10°C/min from room temperature up to 500°C under nitrogen flow.

The tensile tests of PCL/TiO_2 nanocomposites were performed with a WDW 3010 tensile tester (Changchun Kexin, China) at a crosshead speed of 10 mm/min. All the composites specimens were hot pressed into dumbbell specimens with effective dimensions of 60 × 5 × 1 mm^3 and the values were averaged three measurements.

RESULTS AND DISCUSSION

The FTIR spectra of untreated TiO_2 and APS-treated TiO_2 nanoparticles are shown in Figure 1. In the spectrum of g-TiO_2 nanoparticles, the band at 612 cm^{-1} is contributed to vibration absorption peak of Ti—O—Ti and the bands at 1654 and 3448 cm^{-1} assign to surface functional groups —OH of nanoparticles. The bands at 1000–1300 cm^{-1} are contributed to O—Si asymmetric flexible vibration.[20] The band at 2963 cm^{-1} assigns to the appearance of alkyl groups [—$(CH_2)_n$—]. Furthermore, the peak at 2963 cm^{-1} still exists after extraction separation for several times reconfirms condensation reaction between methoxy groups of APS and the TiO_2 surface hydroxyl groups. As a result, the surface modification of TiO_2 nanoparticles by APS is carried out successfully.

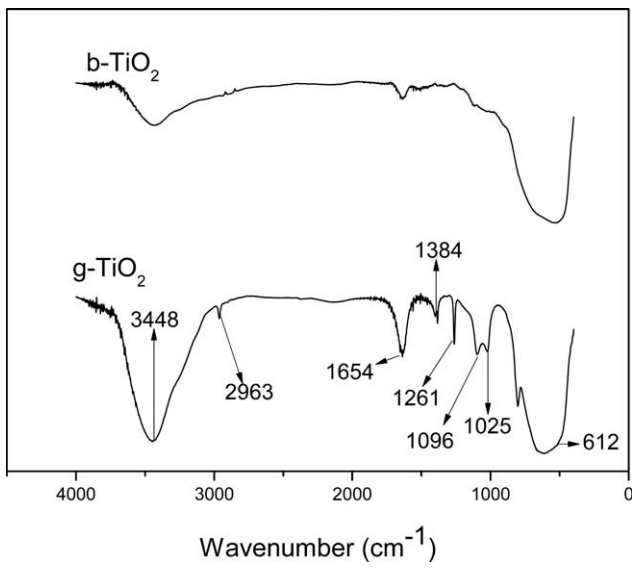

Figure 1 FTIR spectra of b-TiO_2 and g-TiO_2 nanoparticles.

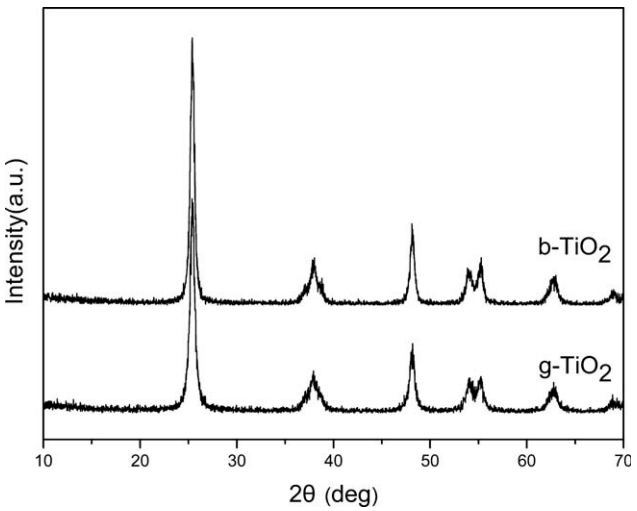

Figure 2 WAXD patterns of b-TiO_2 and g-TiO_2 nanoparticles.

The WAXD patterns of b-TiO_2 and g-TiO_2 nanoparticles are shown in Figure 2. The b-TiO_2 nanoparticles exhibit several characteristic peaks at $2\theta = 25.5°$, 38.1°, 48.1°, and 55.2°, which are consistent with the crystalline nature of TiO_2 nanoparticles. Also, the diffraction peak of maximum intensity appears at $2\theta = 25.5°$, which is in accordance with the characteristic diffraction peak of anatase TiO_2 particles.[21] For g-TiO_2 nanoparticles, it shows an almost similar pattern compared with that of bare TiO_2 nanoparticles, indicating that the grafting reaction does not cause any crystalline change as well as additional secondary phase. According to the Scherrer equation, $d = k\lambda/\cos\theta$, where d is the particle size of TiO_2 nanoparticles, λ is the wavelength of the X-ray, b is the half-peak width of the diffraction peak, k is a constant, and θ is the half diffraction angle, the size of the untreated TiO_2 particles and modified TiO_2 particle is about 20 nm.

The TEM measurements were carried out to confirm the particle size and morphology of TiO_2 and modified TiO_2 nanoparticles more clearly. Figure 3 represents the TEM images of the b-TiO_2 and g-TiO_2 nanoparticles dispersed in chloroform. It can be seen from Figure 3(a) that the nearly spherical bare TiO_2 nanoparticles with a diameter of 20–30 nm, which is consistent with the product description of TiO_2

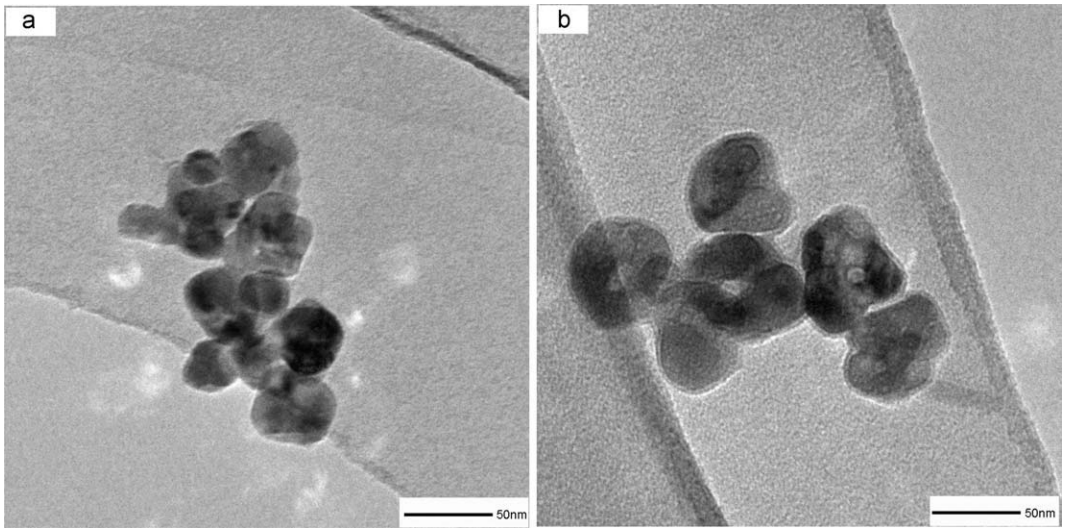

Figure 3 TEM micrographs of b-TiO_2 nanoparticles (a) and g-TiO_2 nanoparticles (b).

nanoparticles and the calculation of WAXD patterns. Figure 3(b) represents g-TiO_2 nanoparticles with visible coupling layers around the particles after being surface modification. In comparison with the initial size of b-TiO_2 nanoparticles, their sizes are slightly big (30–40 nm), due to the existence of coupling shell. This may be explained that the WAXD pattern is generally used to calculate the size of crystal lattice, which is different with the size of nanoparticles.

Figure 4 shows the schematic of the process of g-TiO_2 nanoparticles and PCL/TiO_2 nanocomposites. First, the nanoparticles were dispersed in butanone, followed by adding APS under ultrasonication. After a while, triethyl amine was utilized to initiate the graft reaction and the hydroxyl groups on the surface of the TiO_2 nanoparticles were reactive sites for the reaction with alkoxy groups of silane compounds. Then, the grafted-TiO_2 nanoparticles were obtained at last. Second, the resulting g-TiO_2 nanoparticles were dispersed in ε-CL monomer and ultrasonicated for a while to obtain well dispersed solution. In this stage, the hydroxyl groups presented on the surface of TiO_2 nanoparticles may react with ε-CL monomer through the way of ROP and the PCL molecules were tethered to the surface of TiO_2 nanoparticles. As a result, the PCL/TiO_2 nanocomposites were obtained successfully.

The composition and the corresponding molecular weight of the PCL/b-TiO_2 and PCL/g-TiO_2 nanocomposites are shown in Table I. The pure PCL has the highest molecular weight and the lowest molecular weight distribution (MWD) compared with the samples in which TiO_2 nanoparticles were added. In this case, the molecular weight of the PCL exhibits a continuous decrease with an increasing TiO_2 loading level, whatever adding b-TiO_2 or g-TiO_2 nanoparticles. This can be attributed to the increasing concentration of the hydroxyl groups that exist in the chemical structure of the surface of the filler, which act as the initiators in the ROP. Moreover, adding

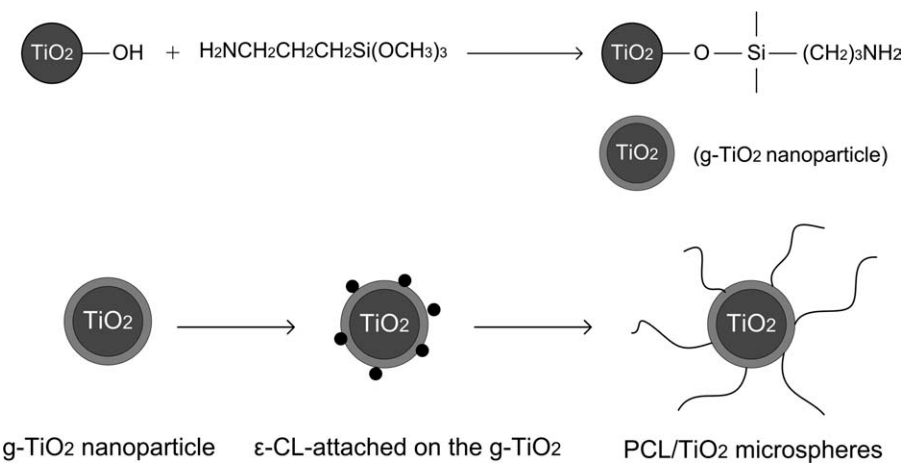

Figure 4 Schematic of the process of g-TiO_2 nanoparticels and PCL/TiO_2 nanocomposites.

TABLE I
Composition and Molecular Weight of PCL/b-TiO_2 and PCL/g-TiO_2 Nanocomposites

TiO_2 content (wt %)[a]		0	1	3	5
M_n[b] (g mol^{-1})	PCL/b-TiO_2	61100	53400	43000	35300
	PCL/g-TiO_2		51600	40700	32600
M_w/M_n[b]	PCL/b-TiO_2	1.26	1.68	1.73	1.82
	PCL/g-TiO_2		1.64	1.71	1.79

[a] Other reaction conditions: $Sn(Oct)_2$: 0.1 wt %, 130°C, 10 h.
[b] Measured by GPC analysis with PS standard calibration, THF was used as eluent at 25°C.

surface-treated nanofiller leads to be a more lightly pronounced decrease in Mn and a concomitant increase in MWD.

WAXD measurements were performed to explore the effects of the addition of b-TiO_2 and g-TiO_2 on the crystal structure of PCL matrix. Figure 5 shows the WAXD patterns of neat PCL, PCL/b-TiO_2, and PCL/g-TiO_2 nanocomposites. Neat PCL shows three main characteristic peaks around $2\theta = 21.4°$, 22.0°, and 23.7°, corresponding to [110], [111], and [200] planes of the orthorhombic crystal form.[22] Moreover, the nanocomposites also exhibit almost the same diffraction peaks at the same locations, indicating that the incorporating of b-TiO_2 or g-TiO_2 does not significantly affect the crystalline structure of PCL matrix. Also, it should be noted that a diffraction peak at $2\theta = 25.5°$ can also be observed for the PCL/b-TiO_2 and PCL/g-TiO_2 nanocomposites, indicating that the crystallization of TiO_2 nanoparticles may occur when they are dispersed in the PCL matrix.

It is clear that the dispersion of nanofiller in the polymer matrix plays an important role in the properties of biodegradable polymers and end use of nanocomposites. Therefore, SEM was employed to explore the morphology of cross-section of films to examine the dispersion of the bare and grafted TiO_2 nanoparticles within the PCL matrix. Figure 6 shows the SEM micrographs of PCL, PCL/b-TiO_2 and PCL/g-TiO_2 nanocomposites. For PCL/b-TiO_2 nanocomposites, it can be seen that the nanocomposites consist of uniform nanoparticles when the content of nanofiller is low, such as 1 and 3 wt %. However, partial much bigger aggregation can be found at higher TiO_2 loading, as indicated in Figure 6(d). For PCL/g-TiO_2 nanocomposites, surface-grafted TiO_2 nanoparticles are well separated and randomly distributed in PCL matrix, even at higher content. This can be explained that surface modification by APS can improve the compatibility between TiO_2 nanoparticles and polymer matrix, which can solve or relieve the appearance of strong aggregation between TiO_2 nanoparticles. What's more, the fracture surface is relatively rough and the TiO_2 nanoparticles are wrapped within the PCL matrix, which indicates that strong interfacial interaction between the matrix and the fillers.

TEM has been proven to be a powerful tool to investigate the dispersion of nanofiller embedded within a polymer matrix. Figure 7 presents the representative TEM micrographs of PCL-b5 and PCL-g5 nanocomposites. It is obvious from the TEM images that the surface modification by the silane agent leads to finer dispersion and distribution of g-TiO_2 nanoparticles. Also, without any surface treatment, some clusters or aggregates of TiO_2 nanoparticles are observed throughout the PCL matrix. These results confirm that the phenomenon of nanoparticles agglomeration decreased effectively due to improved compatibility between TiO_2 nanoparticles and PCL matrix by the introduction of surface modification.

It is wellknown that PCL is a kind of typical semicrystalline polymers, and the crystallization behavior of PCL significantly influences not only the crystalline structure and morphology but also the resulting mechanical properties. Thus, it is of importance to investigate the crystallization behavior both from the theoretical and practical points of view. DSC crystallization exotherms for PCL/b-TiO_2 and PCL/g-TiO_2 nanocomposites are shown in Figure 8, and the thermal and crystallization properties determined from DSC runs are summarized in Table II. It is obvious that the addition of TiO_2 nanofillers, surface treated or not, allows for increasing the crystallization temperature (T_c) of the PCL matrix, showing a heterogeneous nucleating effect of the nanoparticles. The increase in the degree of T_c are more pronounced for the nanocomposites obtained using g-TiO_2 nanoparticles with respect to b-TiO_2 nanofiller, indicating a stronger heterogeneous nucleating effect of g-TiO_2

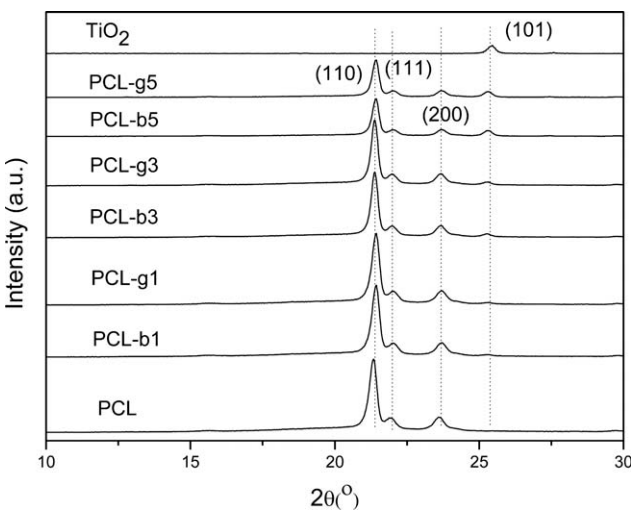

Figure 5 WAXD patterns of PCL/b-TiO_2 and PCL/g-TiO_2 nanocomposites.

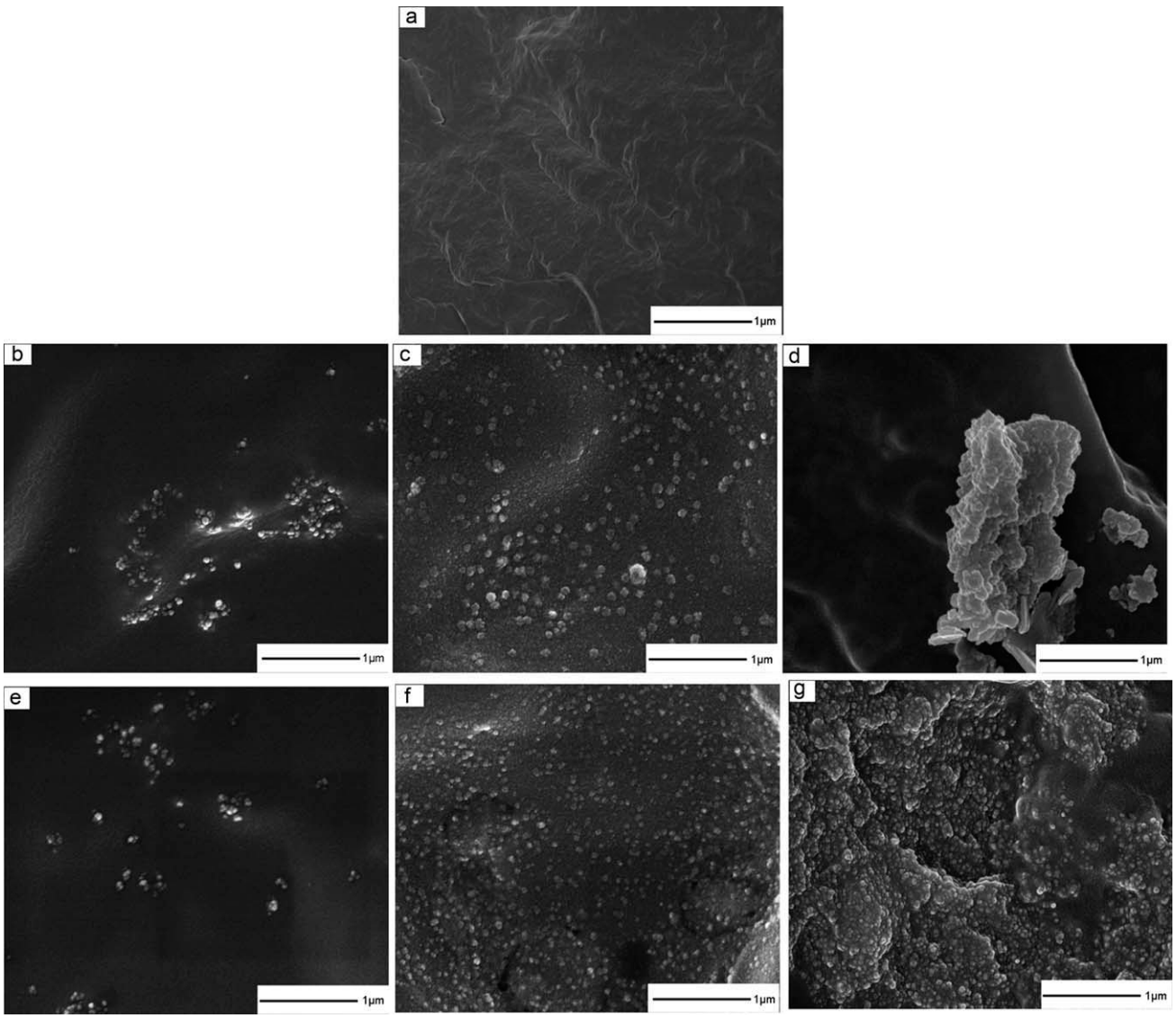

Figure 6 SEM images of cross-sections from pure PCL (a), PCL-b1 (b), PCL-b3 (c), PCL-b5 (d), PCL-g1 (e), PCL-g3 (f), and PCL-g5 (g) nanocomposites.

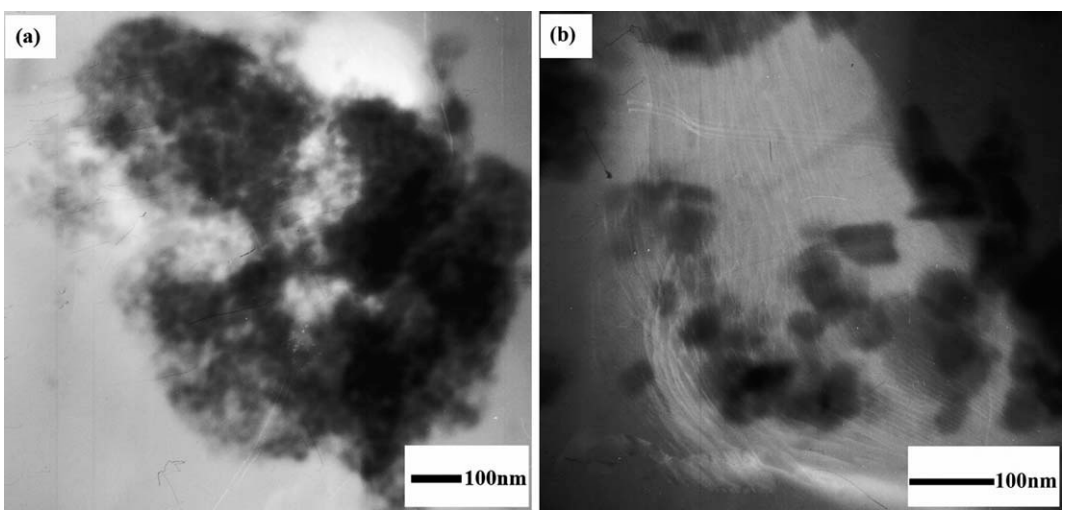

Figure 7 Representative TEM microphotographs of PCL-b5 (a) and PCL-g5 (b) nanocomposites.

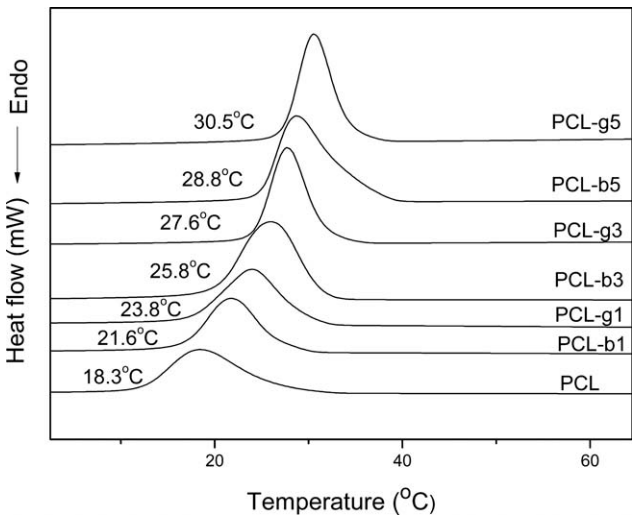

Figure 8 DSC traces of PCL/b-TiO_2 and PCL/g-TiO_2 nanocomposites.

nnaoparticles. The introduction of surface modification endows TiO_2 nanoparticles with better compatibility between TiO_2 nanoparticles and PCL matrix, which makes PCL chain segments more easily to tie to the surface of the TiO_2 nanoparticles. As a result, the primary crystallization of PCL is promoted and the energy needed is reduced, which leads to the decrease of supercooling and the corresponding increase of crystallization temperature. It should be noticed that the addition of surface-treated TiO_2 nanoparticles does not significantly change the melting temperature (T_m) of PCL matrix (neat PCL shows the T_m at 59.8°C, nanocomposites containing g-TiO_2 which reveals at 55–57°C), while the T_m is kept in a similar interval (56–58°C) of PCL/b-TiO_2 nanocomposites. Also, it is found that the crystallinity of PCL slightly increases with the increasing of b-TiO_2 or g-TiO_2 loading. Moreover, the crystallinity degree of the PCL matrix are of more importance for the PCL/g-TiO_2 nanocomposites with respect to PCL/b-TiO_2 nanocomposites.

TABLE II
Thermal and Crystalline Properties of PCL/b-TiO_2 and PCL/g-TiO_2 Nanocomposites

Sample	ΔH_c (J/g)	ΔH_m (J/g)	T_m[a] (°C)	X_c[b] (%)
PCL	55.8	47.7	59.8	34.2
PCL-g1	59.7	53.5	58.4	38.7
PCL-g3	64.7	61.4	57.2	45.4
PCl-g5	79.3	72.1	56.7	54.4
PCL-b1	57.8	51.4	57.9	37.2
PCL-b3	62.1	56.1	56.4	41.6
PCL-b5	66.0	63.1	55.7	47.6

[a] T_m are taken at the maximum of the melt peaks.
[b] $X_c = \Delta H_m/(1 - \&)\Delta H_o$, ΔH_m is the melting enthalpy; & is the mass fraction of TiO_2 particles; ΔH_o is the ΔH_m for 100% crystalline PCL, i.e., 139.5 J/g[3].

TABLE III
Thermal Stability of PCL/b-TiO_2 and PCL/g-TiO_2 Nanocomposites

Sample	Composition (wt %) Nanofiller type	Temperature[a] (°C) b-TiO_2	Temperature[a] (°C) g-TiO_2	Temperature[b] (°C) b-TiO_2	Temperature[b] (°C) g-TiO_2
1	0% TiO_2	335		424	
2	1% TiO_2	358	368	426	432
3	3% TiO_2	364	383	430	448
4	5% TiO_2	373	399	436	457

[a] Temperature for 5 wt % weight loss.
[b] Temperature of maximum rate of degradation (°C) (from D-TG).

To examine the comparative effect of b-TiO_2 and g-TiO_2 addition on the thermal stability of PCL, TGA measurements were carried out on neat PCL and nanocomposite samples. Table III shows the thermographic analysis data of 5% weight loss ($T_{5\%}$) and of the temperature corresponding to the maximum rate of thermal degradation (T_D from D-TG). It is interesting to mention that $T_{5\%}$ is often considered to be the initial decomposition temperature.[23] It comes out that, for both PCL/TiO_2 nanocomposites, adding untreated TiO_2 nanoparticles or surface-treated TiO_2 nanoparticles results in an increase in $T_{5\%}$ and T_D compared to the pure PCL matrix. Moreover, it should be noted that the increase in thermal stability is in direct correlation with the content of nanofiller. It is of worth mentioning that in all samples the corresponding nanocomposites obtained using g-TiO_2 nanoparticles, that is, surface-treated TiO_2, are characterized by better thermal performances than those obtained using untreated TiO_2, there exists similar tendencies regarding the increase in $T_{5\%}$ or T_D values with the increase in nanofiller loading. For instance, $T_{5\%}$ and T_D of PCL-g5 nanocomposites is 26°C and 21°C higher than the samples containing untreated nanofiller. Such improvement can be attributed to the well dispersion of g-TiO_2 nanoparticles within the PCL matrix and strong interaction between surface-treated TiO_2 nanoparticles and PCL chains.

It is evident that the interface between the TiO_2 nanoparticles and the polyester matrix plays an important role in the structure–property relationship. Interfacial affinity has been found to be one of the most important factors in determining the mechanical properties of nanocomposites.[24,25] Table IV gathers the mechanical properties of pure PCL compared to nanocomposites containing increasing loading of nanoparticles, surface treated or not. It is obvious that PCL/b-TiO_2 and PCL/g-TiO_2 nanocomposites exhibit a higher tensile strength and Young's modulus but lower ductility with respect to neat PCL matrix. Moreover, for PCL/b-TiO_2 nanocomposites, the

TABLE IV
Mechanical Properties of PCL/b-TiO_2 and PCL/g-TiO_2 Nanocomposites

Sample	Tensile strength (MPa)	Young's modulus (MPa)	Elongation at break (%)
PCL	13.5 ± 0.3	207 ± 13	524 ± 13
PCL-b1	14.7 ± 0.2	247 ± 10	446 ± 15
PCL-b3	15.4 ± 0.1	336 ± 15	332 ± 11
PCL-b5	13.2 ± 0.5	314 ± 16	158 ± 14
PCL-g1	15.7 ± 0.4	293 ± 12	468 ± 13
PCL-g3	17.9 ± 0.7	378 ± 11	367 ± 10
PCL-g5	18.4 ± 0.4	431 ± 15	279 ± 12

addition of surface-treated TiO_2 nanoparticles leads to an important increase in the tensile strength and Young's modulus compared to nanocomposites containing untreated TiO_2 nanofiller. For example, nanocomposites filled 3 wt % surface-treated TiO_2 nanoparticles show excellent mechanical properties, that is, a tensile strength of 17.9 MPa, value that is 16.4% higher than that (15.4 MPa) obtained for the nanocomposites using untreated TiO_2 nanofiller. The improvement in mechanical properties which indicating that the PCL/TiO_2 interface can be tuned by modification with APS coupling agent, could be attributed to the enhancement of the interaction and adhesion between the TiO_2 nanoparticles and the PCL matrix as well as uniform dispersion of the g-TiO_2 nanoparticles. The coating of APS coupler has been formed on the surface of TiO_2 nanoparticles, which results in core-shell structure. It is assumed that the grafted shell serves as the stabilizing component, which hinders the occurrence of agglomeration and thus improves the dispersibility of the nanoparticles within the PCL matrix. Meanwhile, the grafted shell petrates into the PCL matrix, mixing and entangling with the PCL chains in the matrix.[24,26] Thus, the interfacial interaction between grafted TiO_2 nanoparticles and PCL matrix is enhanced greatly, which increase stress transfer to the g-TiO_2 nanoparticles, resulting in higher tensile strength and Young's modulus of the PCL/g-TiO_2 nanocomposites. Also, it should be noted that, for PCL/b-TiO_2 nanocomposites, the tensile strength and Young's modulus of the nanocomposites decrease when the nanofiller content of b-TiO_2 is beyond 3 wt %. This can be explained that the seriously agglomeration of b-TiO_2 nanoparticles occurred, which can be confirmed from the previous SEM images. The agglomeration could be stress concentration points and suppressed interfacial interaction effect, the mechanical properties decreased consequently. The elongation at break of nanocomposites decreases with the increase of nanopaticles content. The PCL/g-TiO_2 nanocomposites exhibit higher elongation at break than the corresponding PCL/b-TiO_2 nanocomposites. The addition of TiO_2 nanoparticles restricts the mobility of PCL chains, as a result, the ductility of nanocomposites decreases.

CONCLUSIONS

In this study, surface of TiO_2 was grafted successfully with APS to modify the dispersion of TiO_2 nanoparticles in PCL matrix. WAXD results showed that the addition of b-TiO_2 or g-TiO_2 did not affect significantly the crystalline structure of PCL matrix. The higher crystallization temperature (T_c) and the crystallinity of TiO_2 particle-composited PCL were obtained using APS-treated TiO_2 nanoparticles compared with untreated TiO_2 nanoparticles. It was found that the molecular weight and MWD of nanocomposites were dependent on the content of the TiO_2 nanoparticles regardless of whether surface-treated modification or not. And the composites with surface-treated TiO_2 by APS have noticeable thermal stability and better mechanical performances, whereas well dispersion of g-TiO_2 on a nanoscale level was revealed by SEM and TEM. The PCL/TiO_2 nanocomposites have a potential of application in biomedical and environmentally friendly fields.

References

1. Griffith, L. G. Acta Mater 2000, 48, 263.
2. Woodruff, M. A.; Hutmacher, D. W. Prog Polym Sci 2010, 35, 1217.
3. Coombes, A. G. A.; Rizzi, S. C.; Williamson, M.; Barralet, J. E.; Downes, S.; Wallace, W. A. Biomaterials 2004, 25, 315.
4. Chen, B.; Evans, J. R. G. Macromolecules 2006, 39, 747.
5. Young, S. K.; Gemeinhardt, G. C.; Sherman, J. W. Polymer 2002, 43, 6101.
6. Chrissafis, K.; Antoniadis, G.; Paraskevopoulos, K. M.; Vassiliou, A.; Bikiaris, D. N. Compos Sci Technol 2007, 67, 2165
7. Qiao, X. Y.; Li W.; Sun, K.; Xu, S.; Chen, X. D. J Appl Polym Sci 2009, 111, 2908.
8. Liao, L.; Zhang C.; Gong, S. Macromol Rapid Commun 2007, 28, 1148.
9. Luduena, L. N.; Vazquez, A.; Alvarez, V. A. J Appl Polym Sci 2008, 109, 3148.
10. Hua, L.; Kai, W. H.; Inoue, Y. J Appl Polym Sci 2007, 106, 4225.
11. Horikoshi, S.; Serpone, N.; Hisamatsu, Y.; Hidaka, H. Environ Sci Technol 1998, 32, 4010.
12. Zan, L.; Wang, S.; Fa, W.; Hu, Y.; Tian, L.; Deng, K. Polymer 2006, 47, 8155.
13. Turton, T. J.; White, J. R. Polym Degrad Stab 2001, 74, 559.
14. Kim, S. H.; Kwak, S. Y.; Suzuki, T. Polymer 2006, 47, 3005.
15. Hagfeldtt, A.; Gratzel, M. Chem Rev 1995, 95, 49.
16. Li, R.; Nie, K. M.; Shen, X. F.; Wang, S. Mater Lett 2007, 61, 1368.
17. Catauto, M.; Raucci, M. G.; de Marco, D.; Ambrosio, L. J Biomed Mater Res A 2006, 77, 340.
18. Li, R.; Nie, K. M.; Pang, W. M.; Zhu, Q. R. J Biomed Mater Res A 2007, 83, 114.

19. Sabzi, M.; Miranedini, S. M.; Zohuriaan-Mehr, J.; Atai, M. Prog Org Coat 2009, 65, 222.
20. Jun, L.; Siddiqui, J. A.; Ottenbrite, R. M. Polym Adv Technol 2001, 12, 285.
21. Thamaphat, K.; Limsuwan, P.; Ngotawornchai, B. Kasetsart J Nat Sci 2008, 42, 357.
22. Xu, G.; Du, L.; Xia, R.; Meng, X.; Zhu, Q. Polym Int 2008, 57, 1052.
23. Carrasco, F.; Pagès, P.; Gámez-Pérez, J.; Santana, O. O.; Maspoch, M. L. Polym Degrad Stab 2010, 95, 2508.
24. Lu, X. L.; Lv, X. Q.; Sun, Z. J.; Zheng, Y. F. Eur Polym J 2008, 44, 2476.
25. Luo, Y. B.; Wen, D. L.; Wang, X. L.; Da, Y. X.; Wang, Y. Z. Acta Mater 2009, 57, 3182.
26. Hong, Z. H.; Zhang, P. B.; He, C. L.; Qiu, X. Y.; Liu, A. X.; Chen, L. Chen, X. S.; Jing, X. B. Biomaterials 2005, 26, 6296.